International Journal of Innovative
Computing, Information and Control
Volume **19**, Number **4**, August **2023**

ICIC International ©2023 ISSN 1349-4198
pp. 1165–1177

DYNAMIC SURFACE CONTROL DESIGN FOR HYBRID EXCITATION SYNCHRONOUS MACHINES

Ekkachai Mujjalinvimut[1] and Adirak Kanchanaharuthai[2,*]

[1]Department of Electrical Engineering
Faculty of Engineering
King Mongkut's University of Technology Thonburi
Pracha Uthit Road, Bang Mod, Bangkok 10140, Thailand
ekkachai.muj@kmutt.ac.th

[2]Department of Electrical Engineering
College of Engineering
Rangsit University
52/347 Muang-Ake, Phaholyothin Road, Lak-Hok, Muang, Patumthai 12000, Thailand
*Corresponding author: adirak@rsu.ac.th

Received December 2022; revised March 2023

Abstract. *In this research, a nonlinear feedback stabilizing controller technique is developed for a hybrid excitation synchronous machine (HESM) system. Utilizing the dynamic surface method, the desired control law is designed. The developed control mechanism ensures that all closed-loop system trajectories are semi-globally uniformly and ultimately bounded. A nonlinear dynamical system of the HESM is used to demonstrate the effectiveness and applicability of the technique. The simulation results indicate that the method can maintain speed even in the presence of a sudden load torque. It is capable of rapidly reducing oscillations and outperforming the existing nonlinear controller such as the backstepping controller.*

Keywords: Nonlinear control, Dynamic surface control, Hybrid excitation synchronous machine

1. **Introduction.** The HESM was initially suggested in [1]. HESM differs structurally from both general excitation synchronous machines and permanent magnet synchronous machines. It has a permanent magnet and field winding, and its two magnetization sources are concurrent. As it combines the benefits of both permanent magnet machines and excitation machines, its development potential is vast. Unfortunately, the HESM is a multivariable, strongly coupled, extremely nonlinear system. The high nonlinearity is a result of the coupling between speed and armature currents, as well as perturbations such as inadequate modeling of uncertain parameters (armature winding resistance, moment of inertia, etc.), sensor errors (angular position, angular velocity), and discretization influences (delay, numerical errors).

HESM has recently gained increased attention and has become one of the new research hotspots as significant effort has been made on energy savings and broad timing drive systems. The vast majority of current HESM research [2, 3, 4] has focused on machine design, manufacturing, and test analysis, with little emphasis on speed regulation. Speed control of electric motors and machinery is ubiquitous in contemporary society, as is well known. The list of devices requiring speed control is extensive, ranging from household electrical appliances used in the garden and garage to large industrial facilities with conveyor belts, pumps, and machine tools. Clearly, the speed control is a direct indicator

DOI: 10.24507/ijicic.19.04.1165

of the machine's operation and is crucial to the quality and outcome of the work. The HESM, however, is a novel structural machine that differs from both general excitation synchronous machines and permanent magnet synchronous machines. Therefore, there is currently no effective method for controlling the HESM's speed. In addition, this research focuses on the development of an advanced nonlinear speed regulation.

Because the HESM system is affine in control, applying nonlinear system geometric theory to it is natural. The key findings are that the HESM system is locally weakly controllable, strongly accessible, and locally weakly observable. It is also input-output invertible and linearizable. As a result, a linear control strategy complements the HESM well. The linear control technique is obtained by precisely removing nonlinear terms that degrade performance. Furthermore, when the equivalent equilibrium point, such as unknown parameters or changing environmental temperatures, is changed, the linear control approach cannot guarantee system stability. As a result, the linear control technique will fail to provide global stability within the scope of the servo drive.

To the author's knowledge, relatively little research has focused on directly applying nonlinear control theory to the development of a feedback stabilizing nonlinear controller for the HESM. To handle nonlinear coupling and parameter uncertainties and make the HESM rotor speed track the desired rotor speed, an adaptive backstepping control design [5] was developed. Even if the resulting controller was effective, finding the ideal controller required choosing the virtual control functions and their derivatives at each stage of the design. A nonlinear $\mathcal{H}_\infty$ controller design [6] for hybrid excited synchronous generators via AC/DC and DC/AC converters has been presented with the aid of approximate linearization around a temporary operating point. In order to control a hybrid excitation synchronous generator motor, in [7], Sun et al. proposed a feedback linearization decoupling sliding mode controller design. The obtained controller improved dynamic responses and decreased torque and current ripples despite load disturbances. However, the feedback linearization method was used in its design.

Even if the aforementioned nonlinear controller design strategies are effective, there are significant drawbacks, according to the aforementioned research. The developed control was created using the linearizing method, which may reduce system performance while changing the operating point, according to the result of [6]. In order to find the desired controller reported in [7], the presented control combined the feedback linearization method with a sliding mode design, which required choosing the output function and the sliding surface function. It is not systematic to choose both functions appropriately, though. Backstepping design, in particular, is centered on determining the final controller by discovering its derivatives in each step, resulting in a systematically developed approach. Although the backstepping approach is a powerful control design technique that has been successfully applied to a number of real-world systems, it has a significant drawback. This drawback is the "explosion of complexity" issue, which results from the repeated differentiations of virtual control functions. It occurs frequently in large-scale systems, making it challenging to compute the time derivative of the virtual control functions at each design procedure. This increases the complexity of the final control law. A concept of dynamic surface control design [9, 10] is proposed to eliminate the problem of repeated differentiations of the virtual control variables in order to overcome this disadvantage. It is observed that such virtual control variables pass via a low-pass filter at each design stage, hence preventing the derivative of virtual control variables.

This research continues this line of investigation and focuses on an advanced nonlinear controller design to make the rotor speed follow the reference rotor speed for the nonlinear HESM model. In this paper, the controller is designed utilizing a dynamic surface control (DSC) method. Finding a stabilizing feedback controller is the control objective of the

DSC control method. The controller developed in this study has a systematic design process and can address the "explosion of complexity" issue brought on by backstepping. Another advantage of using DSC is that it considerably relaxes the requirement for the smoothness of plant functions and the desired signal. As a result, the DSC technique has been used to construct simplified nonlinear feedback stabilizing as well as adaptive controllers for uncertain nonlinear systems. In addition, the DSC control design has been effectively applied to a wide range of practical systems [12, 13, 14, 15].

As discussed previously, the following are the primary contributions of this work.

- Using a nonlinear HESM dynamic model, it is suggested that a dynamic surface control method be used to solve the previously unexplored HESM speed tracking control problem.
- The closed-loop system's signals are all semi-globally uniformly and ultimately bounded thanks to Lyapunov theory, which also enables asymptotic tracking based on a suitable selection of the design parameters.

The rest of this paper is organized as follows. Section 2 is a brief presentation of dynamic model of the HESM system and the problem statement. Nonlinear dynamic surface control design is provided in Section 3. In Section 4, the simulation results are given to show the effectiveness of the developed design. Finally, the paper is concluded in Section 5.

2. **HESM System Model.** The hybrid excitation synchronous machine [5, 7] is characterized by the following dynamical equations in the synchronously rotating rotor's d-q coordinates:

$$\begin{cases} \dot{\omega} = \dfrac{R_\Omega}{J}\omega + \dfrac{P_n}{J}\left(L_d - L_q\right) i_q i_d + \dfrac{P_n \Phi_a}{J} i_q + \dfrac{P_n M_f}{J} i_q i_f - \dfrac{1}{J} T_l, \\ \dot{i}_d = -L_f R K i_d + L_f L_q K P_n \omega i_q + M_f R_f K i_f + L_f K u_d - M_f K u_f, \\ \dot{i}_q = \dfrac{-L_d}{L_q} P_n \omega i_d - \dfrac{R}{L_q} i_q - \dfrac{M_f}{L_q} P_n \omega i_f - \dfrac{\Phi_a}{L_q} P_n \omega + \dfrac{1}{L_q} u_q, \\ \dot{i}_f = -M_f R K i_d - M_f L_q K P_n \omega i_q - L_f R_f K i_f - M L_f K u_d - L_d K u_f \end{cases} \tag{1}$$

with $K = \frac{1}{L_d L_f - M_f^2}$, where u_d, u_q, and u_f denote the d- and q-axes stator, and auxiliary excitation winding voltages, respectively. i_d, i_q, and i_f denote d- and q-axes stator, and auxiliary excitation winding currents, respectively. R and R_f represent stator per-phase and auxiliary excitation winding resistances, respectively; L_d, L_q, and L_f are d- and q-axes stator, and auxiliary excitation winding inductances, respectively; M_f denotes the mutual induction between auxiliary excitation winding and d-axis winding; Φ_a represents the flux linkage of rotor permanent-magnet; P_n denotes the number of poles of the machine; ω denotes the rotor speed in angular frequency; J represents the moment of inertia of the machine and load; R_Ω is the friction coefficient of the machine; and T_l represents the load torque.

Remark 2.1. *In this study, it can be seen that the load torque T_l, friction coefficient R_Ω, and moment of inertia J have constant values. However, these parameters are unknown in HESM systems in practice. For the sake of simplicity, the authors assumed that they were constants while developing the dynamic surface controller. For future work, an adaptive dynamic surface control design will be designed to estimate these unknown parameters.*

It is clear that the HESM model contains the input variables u_d, u_q, and u_f. The HESM system, which is managed by the voltage source, can use these variables. The model's inputs are affine, and the first subsystem of (1) contains no inputs.

Firstly, let us introduce the following state variables to simplify the system's state-space equation:

$$x_1 = \omega - \omega_r,\ x_2 = i_d,\ x_3 = i_q,\ x_4 = i_f, \tag{2}$$

where ω_r denotes the reference input which needs to be tracked.

Therefore, the state variable vector used in this design procedure is denoted as $x = [x_1, x_2, x_3, x_4]^T$. The dynamic model of the nonlinear HESM system can be rewritten as an affine nonlinear system as follows after differentiating the state variables mentioned above:

$$\dot{x} = f(x) + g(x)u(x) \tag{3}$$

with

$$f(x) = \begin{bmatrix} f_1(x) \\ f_2(x) \\ f_3(x) \\ f_4(x) \end{bmatrix} = \begin{bmatrix} -\dfrac{R_\Omega}{J}(x_1+\omega_r) + \dfrac{P_n}{J}(L_d - L_q)x_2x_3 + \dfrac{P_n\Phi_a}{J}x_3 + \dfrac{P_nM_f}{J}x_3x_4 - \dfrac{T_l}{J} \\ -L_fRKx_2 + L_fL_qKP_n\omega x_3 \\ \dfrac{-L_d}{L_q}P_n\omega x_2 - \dfrac{R}{L_q}x_3 - \dfrac{M_f}{L_q}P_n\omega x_4 - \dfrac{\Phi_a}{L_q}P_n\omega \\ M_fRKx_2 - M_fL_qKP_n\omega x_3 - L_fR_fKx_4 \end{bmatrix},$$

$$g(x) = \begin{bmatrix} 0 & 0 & 0 \\ g_{21}(x) & 0 & g_{23}(x) \\ 0 & g_{32}(x) & 0 \\ g_{41}(x) & 0 & g_{43}(x) \end{bmatrix} = \begin{bmatrix} 0 & 0 & 0 \\ L_fK & 0 & -M_fK \\ 0 & \dfrac{1}{L_q} & 0 \\ -M_fK & 0 & L_dK \end{bmatrix},\ u(x) = \begin{bmatrix} u_d \\ u_q \\ u_f \end{bmatrix}. \tag{4}$$

In addition, the region of operation is defined in the set $\mathcal{D} = \{x \in \mathbb{R}\times\mathbb{R}\times\mathbb{R}\times\mathbb{R}\}$. The open loop operating equilibrium is denoted by $x_e = [x_{1e}, x_{2e}, x_{3e}, x_{4e}]^T = [0, i_{de}, i_{qe}, i_{fe}]^T$.

The following assumption, definition, and lemmas are established in order to satisfy these required objectives above.

Assumption 2.1. *All state variables $x_1, x_2, x_3, x_4 \in \mathbb{R}$, are assumed to be measurable.*

Remark 2.2. *In this work, the authors assumed that all states are measured only for the sake of simplicity to design the dynamic surface controller. In future work, we will propose an output feedback controller via dynamic surface control design.*

Definition 2.1. *Consider the nonlinear system*

$$\dot{x}(t) = f(x,t),$$

where $x(t) \in R^n$ is the state vector. Its solution is said to be semi-global uniformly and ultimately bounded (SGUUB) if, for $x(0) \in \Omega_x$ which is a compact set, there exist two constants σ and $T(\sigma, x(0))$, such that $\|x(t)\| \le \sigma$ is held for all $t > t + T(\sigma, x(0))$.

Lemma 2.1. [8] *If the constants $p > 1$ and $q > 1$ are such that $(p-1)(q-1) = 1$, then for all $\epsilon > 0$ and all $(x, y) \in \mathbb{R}^2$ we have*

$$xy \le \frac{\epsilon^p}{p}|x|^p + \frac{1}{q\epsilon^q}|y|^q. \tag{5}$$

If choosing $p = q = 2$ and $\epsilon^2 = 2\kappa$, the inequality above becomes

$$xy \le \kappa x^2 + \frac{1}{4\kappa}y^2. \tag{6}$$

For simplicity, provided that $\kappa = \frac{1}{2}$, it is straightforward to obtain the following inequality

$$xy \leq \frac{x^2}{2} + \frac{y^2}{2}. \tag{7}$$

Lemma 2.2. [8] *Let $\mathcal{V}(t) \in R$ be a non-negative function of time on $[0, +\infty)$ which satisfies the differential inequality*

$$\dot{\mathcal{V}} \leq a\mathcal{V} + b, \tag{8}$$

where $a \in R$ and $b \in R$ are positive constants. Then the function $\mathcal{V}(t)$ satisfies the following inequality:

$$\mathcal{V}(t) \leq e^{-at}\mathcal{V}(0) + \frac{b}{a}\left(1 - e^{-at}\right), \ \forall t \in [0, +\infty). \tag{9}$$

Additionally, when time approaches infinity, $\mathcal{V}(t)$ will become $\frac{b}{a}$.

Problem statement: The goal of this paper is to use the dynamic surface control method to develop a nonlinear control voltage $u(x)$ for the HESM model. The developed controller meets the following requirements: (i) The HESM rotor speed ω can track the desired rotor speed ω_r, and (ii) The overall closed-loop system trajectories are semi-global uniformly and ultimately bounded.

To obtain a feedback-stabilizing nonlinear control, a dynamic surface control design will be developed for the next section's developed design procedure. The developed control is designed step-by-step to achieve the desired performance in the subsequent section.

3. Nonlinear Control Design.

The concepts of a dynamic surface control strategy are introduced in this section. The nonlinear stabilizing feedback control algorithm for the HESM model is established in this section. The following two subsections go into detail about the significant advancements. The first subsection describes the dynamic surface control technique. The second examines closed-loop system stability using Lyapunov control theory.

3.1. DSC control design.

The proposed control procedure is developed step by step as follows.

Step 1: First, we focus on the first subsystem (3) and (4), and then let us define the error surface $S_1 = x_1 - x_d$. In order to accomplish stability for the error surface S_1, differentiating S_1 with respect to time yields

$$\dot{S}_1 = -\frac{R_\Omega}{J}(x_1 + \omega_r) + \frac{P_n}{J}(L_d - L_q)x_2x_3 + \frac{P_n\Phi_a}{J}x_3 + \frac{P_nM_f}{J}x_3x_4 - \frac{T_l}{J} - \dot{x}_{1d}. \tag{10}$$

From (10), the state variables x_2, x_3 and x_4 are viewed as virtual control inputs; therefore, the desired feedback controllers α_2, α_3, α_4 are be selected as

$$\alpha_2 = \frac{J}{3P_n(L_d - L_q)}\left(-k_1S_1 + \dot{x}_{1d} + \frac{T_l}{J} + \frac{R_\Omega}{J}(x_1 + \omega_r)\right), \tag{11}$$

$$\alpha_3 = \frac{J}{3P_n\Phi_a}\left(-k_1S_1 + \dot{x}_{1d} + \frac{T_l}{J} + \frac{R_\Omega}{J}(x_1 + \omega_r)\right), \tag{12}$$

$$\alpha_4 = \frac{J}{3P_nM_f}\left(-k_1S_1 + \dot{x}_{1d} + \frac{T_l}{J} + \frac{R_\Omega}{J}(x_1 + \omega_r)\right), \tag{13}$$

where k_1 is a positive design constant. Let us introduce new state variables x_{2d}, x_{3d}, x_{4d} and let α_2, α_3, α_4 pass through the following three first-order filters with time constants τ_2, τ_3 and τ_4 to obtain the dynamics of x_{2d}, x_{3d}, x_{4d}:

$$\tau_2\dot{x}_{2d} + x_{2d} = \alpha_2, \ x_{2d}(0) = \alpha_2(0) \Rightarrow \dot{x}_{2d} = \frac{\alpha_2 - x_{2d}}{\tau_2}, \tag{14}$$

$$\tau_3\dot{x}_{3d} + x_{3d} = \alpha_3,\ x_{3d}(0) = \alpha_3(0) \Rightarrow \dot{x}_{3d} = \frac{\alpha_3 - x_{3d}}{\tau_3}, \tag{15}$$

$$\tau_4\dot{x}_{4d} + x_{4d} = \alpha_4,\ x_{4d}(0) = \alpha_4(0) \Rightarrow \dot{x}_{4d} = \frac{\alpha_4 - x_{4d}}{\tau_4}. \tag{16}$$

Step 2: Define the second surface, the third surface, and the fourth surface as

$$S_2 = x_2x_3 - x_{2d}, \tag{17}$$

$$S_3 = x_3 - x_{3d}, \tag{18}$$

$$S_4 = x_3x_4 - x_{4d}. \tag{19}$$

Then, by calculating the derivative of (17)-(19), we have

$$\begin{aligned}
\dot{S}_2 &= \dot{x}_2x_3 + x_2\dot{x}_3 - \dot{x}_{2d} \\
&= (f_2(x) + g_{21}u_d + g_{23}(x)u_f)x_3 + (f_3(x) + g_{32}(x)u_q)x_2 - \dot{x}_{2d} \\
&= -k_2S_2, \qquad (20)\\
\dot{S}_3 &= f_3(x) + g_{32}(x)u_q - \dot{x}_{3d} = -k_3S_3, \qquad (21)\\
\dot{S}_4 &= \dot{x}_3x_4 + x_3\dot{x}_4 - \dot{x}_{4d} \\
&= (f_3(x) + g_{32}(x)u_q)x_4 + x_3(f_4(x) + g_{41}(x)u_d + g_{43}(x)u_f) - \dot{x}_{4d} \\
&= -k_4S_4, \qquad (22)
\end{aligned}$$

where k_2, k_3 and k_4 are positive design constants. Also, $\dot{x}_{2d}$, $\dot{x}_{3d}$, and $\dot{x}_{4d}$ can be directly computed from (14)-(16).

Step 3: Finally, after defining the second, the third and the fourth surfaces in Step 2, we have the time derivative of S_2, S_3 and S_4 along the system trajectories as shown in (20)-(22). Therefore, a suitable selection of the control laws (u_d, u_f, u_q) to achieve the stability is given as follows:

$$\begin{cases}
u_d = -\dfrac{1}{x_3\left(KM_f^2 - KL_dL_q\right)}\left(L_dv_1 + M_fv_2\right), \\
u_f = -\dfrac{1}{KM_f^2 - KL_dL_q}\left(M_fv_1 + L_fv_2\right), \\
u_q = \dfrac{1}{g_{32}(x)}\left[-k_3S_3 - f_3(x) + \dfrac{\alpha_3 - x_{3d}}{\tau_3}\right],
\end{cases} \tag{23}$$

where $v_1 = -k_2S_2 - f_2(x)x_3 - x_2f_3(x) - x_2g_{32}(x)u_q + \frac{\alpha_2 - x_{2d}}{\tau_2}$ and $v_2 = -k_4S_4 - x_4f_3(x) - x_3f_4(x) - g_{32}(x)x_4u_q + \frac{\alpha_4 - x_{4d}}{\tau_4}$. For simplicity, it is observed that the functions $f_2(x)$, $f_3(x)$, $f_4(x)$, and $g_{32}(x)$ are obtained from (3) and (4).

3.2. **Stability analysis.** This subsection examines the stability analysis for the proposed scheme. This section's goal is to prove that the closed-loop system possesses the property of semi-globally uniformly and uniformly ultimate boundedness. First, consider the surface and boundary layer errors' time derivatives as follows:

$$\begin{cases}
\dot{S}_1 = -k_1S_1 + \mathcal{P}_2(S_2 + e_2) + \mathcal{P}_3(S_3 + e_3) + \mathcal{P}_4(S_4 + e_4), \\
\dot{S}_2 = -k_2S_2, \\
\dot{S}_3 = -k_3S_3, \\
\dot{S}_4 = -k_4S_4, \\
\dot{e}_k = -\dfrac{e_k}{\tau_k} + B_k(S_1, \ldots, S_k, e_2, \ldots, e_k),\ k = 2, 3, 4.
\end{cases} \tag{24}$$

where $\mathcal{P}_2 = \frac{P_n(L_d - L_q)}{J}$, $\mathcal{P}_3 = \frac{P_n \Phi_a}{J}$, $\mathcal{P}_4 = \frac{P_n M_f}{J}$. Also, $e_k = x_{kd} - \alpha_k$ is the boundary layer error. $B_k(\cdot)$ is a continuous function defined as follows:

$$\begin{cases} B_2(\cdot) = -\dot{\alpha}_2 = -\dfrac{\partial \alpha_2}{\partial x_1}\dot{x}_1 - \dfrac{\partial \alpha_2}{\partial x_{1d}}\dot{x}_{1d} - \dfrac{\partial \alpha_2}{\partial \omega_r}\dot{\omega}_r, \\ B_3(\cdot) = -\dot{\alpha}_3 = -\dfrac{\partial \alpha_3}{\partial x_1}\dot{x}_1 - \dfrac{\partial \alpha_3}{\partial x_{1d}}\dot{x}_{1d} - \dfrac{\partial \alpha_3}{\partial \omega_r}\dot{\omega}_r, \\ B_4(\cdot) = -\dot{\alpha}_4 = -\dfrac{\partial \alpha_4}{\partial x_1}\dot{x}_1 - \dfrac{\partial \alpha_4}{\partial x_{1d}}\dot{x}_{1d} - \dfrac{\partial \alpha_4}{\partial \omega_r}\dot{\omega}_r. \end{cases} \tag{25}$$

Therefore, the HESM model's dynamic control design can be summed up as follows.

Theorem 3.1. *Under Assumption 2.1, consider the closed-loop dynamics consisting of the HEMS (3) and (4) and the control law (23). If there exists a set of suitable design parameters k_i, c_k ($i = 1, 2, 3, 4$, $k = 2, 3, 4$) satisfying*

$$\begin{cases} \bar{k}_1 = k_1 - \mathcal{P}_2^2 - \mathcal{P}_3^2 - \mathcal{P}_4^2 > 0,\ \bar{k}_2 = k_2 - 0.5 > 0,\ \bar{k}_3 = k_3 - 0.5 > 0,\ \bar{k}_4 = k_4 - 0.5 > 0, \\ \bar{c}_2 = \dfrac{1}{\tau_2} - \dfrac{\bar{B}_2^2}{2\pi_2} - \dfrac{1}{2} > 0,\ \bar{c}_3 = \dfrac{1}{\tau_3} - \dfrac{\bar{B}_3^2}{2\pi_3} - \dfrac{1}{2} > 0,\ \bar{c}_4 = \dfrac{1}{\tau_4} - \dfrac{\bar{B}_4^2}{2\pi_4} > 0, \end{cases} \tag{26}$$

such that all trajectories of the overall closed-loop dynamics are semi-globally uniformly and ultimately bounded.

Proof: We define the Lynapunov function as

$$V = \sum_{j=1}^{4} V_j + \sum_{k=2}^{4} \frac{1}{2} e_k^2. \tag{27}$$

The time derivative of V along trajectories (24) is as follows:

$$\begin{aligned} \dot{V} &= \sum_{i=1}^{4} S_i \dot{S}_i + \sum_{k=2}^{4} e_k \dot{e}_k \\ &= S_1 \left(-k_1 S_1 + \mathcal{P}_2(S_2 + e_2) + \mathcal{P}_3(S_3 + e_3) + \mathcal{P}_4(S_4 + e_4)\right) - k_2 S_2^2 - k_3 S_3^2 - k_4 S_4^2 \\ &\quad + \sum_{k=2}^{4} e_k \left(-\frac{e_k}{\tau_k} + B_k\right). \end{aligned} \tag{28}$$

For $j = 1, 2, 3, 4$, $k = 2, 3, 4$ and $p > 0$, the set $\Omega := \sum_{j=1}^{4} V_j + \sum_{k=2}^{4} e_k^2 \leq 2p$ is compact set in R^7. According to the property of continuous function, we know that $B_k(\cdot)$ has a bound on Ω, such that $|B_k(\cdot)| \leq \bar{B}_k$, $k = 2, 3, 4$. Based on the Young's inequality (Lemma 2.1), we have the following inequalities:

$$\mathcal{P}_2 S_1 S_2 \leq \frac{\mathcal{P}_2^2 S_1^2}{2} + \frac{S_2^2}{2},\ \mathcal{P}_2 S_1 e_2 \leq \frac{\mathcal{P}_2^2 S_1^2}{2} + \frac{e_2^2}{2}, \tag{29}$$

$$\mathcal{P}_3 S_1 S_3 \leq \frac{\mathcal{P}_3^2 S_1^2}{2} + \frac{S_3^2}{2},\ \mathcal{P}_3 S_1 e_3 \leq \frac{\mathcal{P}_3^2 S_1^2}{2} + \frac{e_3^2}{2}, \tag{30}$$

$$\mathcal{P}_4 S_1 S_4 \leq \frac{\mathcal{P}_4^2 S_1^2}{2} + \frac{S_4^2}{2},\ \mathcal{P}_4 S_1 e_4 \leq \frac{\mathcal{P}_4^2 S_1^2}{2} + \frac{e_4^2}{2}, \tag{31}$$

$$e_k \left(-\frac{e_k}{\tau_k} + B_k\right) \leq -\left(\frac{1}{\tau_k} - \frac{\bar{B}_k^2}{2\pi_k}\right) e_k^2 + \frac{\pi_k}{2},\ k = 2, 3, 4. \tag{32}$$

From the inequalities above, one has

$$\dot{V} = -\left(k_1 - \mathcal{P}_2^2 - \mathcal{P}_3^2 - \mathcal{P}_4^2\right) S_1^2 - (k_2 - 0.5) S_2^2 - (k_3 - 0.5) S_3^2 - (k_4 - 0.5) S_4^2$$

$$-\sum_{k=2}^{4}\left(\frac{1}{\tau_k}-\frac{\bar{B}_k^2}{2\pi_3}-\frac{1}{2}\right)e_k^2+\sum_{k=2}^{4}\frac{\pi_k}{2}. \tag{33}$$

After selecting $\bar{k}_1 = k_1 - \mathcal{P}_2^2 - \mathcal{P}_3^2 - \mathcal{P}_4^2 > 0$, $\bar{k}_2 = k_2 - 0.5 > 0$, $\bar{k}_3 = k_3 - 0.5 > 0$, $\bar{k}_4 = k_4 - 0.5 > 0$, $\bar{c}_2 = \frac{1}{\tau_2} - \frac{\bar{B}_2^2}{2\pi_2} - \frac{1}{2} > 0$, $\bar{c}_3 = \frac{1}{\tau_3} - \frac{\bar{B}_3^2}{2\pi_3} - \frac{1}{2} > 0$, $\bar{c}_4 = \frac{1}{\tau_4} - \frac{\bar{B}_4^2}{2\pi_4} - \frac{1}{2} > 0$, we obtain

$$k = \min\left\{\bar{k}_1, \bar{k}_2, \bar{k}_3, \bar{k}_4, \bar{c}_2, \bar{c}_3, \bar{c}_4\right\} > 0. \tag{34}$$

After that, the following inequalities hold.

$$\dot{V} \leq -kV + \Pi. \tag{35}$$

After solving Inequality (35) and using Lemma 2.2, we obtain

$$0 \leq V(t) \leq \left(V(0) - \frac{\Pi}{c}\right)e^{-ct} + \frac{\Pi}{c}. \tag{36}$$

From (36), it can be inferred that $V(t)$ eventually settles down to $\frac{\Pi}{c}$. This means that all the trajectories of the closed-loop dynamics are semi-globally uniformly ultimately bounded. In particular, it implies that S_i, e_k are all semi-globally uniformly ultimately bounded. This completes the proof.

4. **Simulation Results.** The performance verification and efficacy of the presented controller are shown in this part. The simulations are used to evaluate the proposed controller. Additionally, the effectiveness of the suggested control method is assessed in MATLAB environment.

This HESM model uses the following physical parameters (pu.), controller parameters, and initial parameters:

- The parameters of the HESM model [5] in (1) are $R = 2.875\ \Omega$, $R_f = 2.5\ \Omega$, $L_d = 0.0085$ H, $L_q = 0.008$ H, $L_f = 0.008$ H, $M_f = 0.0025$ H, $R_\Omega = 0.0002$ Nms, $P_n = 2$, $\Phi_A = 0.175$ Wb, $J = 0.0008$ kg·m^2, $\omega_r = 500$ rad/s.
- The control parameters of the proposed controller are $k_1 = 20$, $k_2 = 0.1$, $k_3 = 10$, $k_4 = 0.1$, $\tau_2 = \tau_3 = \tau_4 = 0.01$.
- Initial parameters $\omega_0 = 1$ rad/s, $I_{d0} = I_{q0} = I_{f0} = 1$ A.

The time domain simulations are carried out via MATLAB environment. To investigate the system dynamic performance of the designed controller, as given in (23), in the system under study. The performance of the proposed controller is compared with that of the backstepping controller [8], as given in (37)

- Backstepping controller (BSC) [8]

$$\begin{cases} u_q(x) = \dfrac{1}{g_{32}(x)}\left(-c_3y_3 - f_3(x) + \dot{\alpha}_3 - \dfrac{P_n\Phi_a z_1}{J}\right), \\ u_d(x) = -\dfrac{1}{\Delta}\left(L_d\bar{v}_1 + M_f\bar{v}_2\right), \\ u_f(x) = -\dfrac{1}{\Delta}\left(M_f\bar{v}_1 + L_f\bar{v}_2\right), \end{cases} \tag{37}$$

where $y_1 = x_1 - \omega_r$, $y_2 = x_2 - \alpha_2$, $y_3 = x_3 - \alpha_3$, $y_4 = x_4 - \alpha_4$, $\alpha_2 = \alpha_4 = 0$, $\alpha_3 = \frac{J}{P_n\Phi_a}\left(-c_1y_1 + \frac{R_\Omega}{J}(z_1+\omega_r) + \frac{T_L}{J}\right)$, $\bar{v}_1 = -c_2y_2 - \frac{P_n}{J}(L_d - L_q)i_qy_1 - f_2(x)$, $\bar{v}_2 = -c_4y_4 - \frac{M_fP_n}{J}i_qy_1 - f_4(x)$, $\Delta = KM_f^2 - KL_dL_f \neq 0$. The controller parameters of the backstepping control law are chosen as follows: $c_i = 20$, $i = 1, 2, 3, 4$.

Moreover, the following load torque was applied in the simulations:

$$T_l = \begin{cases} 0.1, & 0 \leq t \leq 0.6 \text{ s}, \\ 1.5, & 0.6 \text{ s} < t \leq 1 \text{ s} \\ 0.1, & 1 \text{ s} < t \leq 1.5 \text{ s} \end{cases}$$

The simulation findings are given and analyzed in the sections that follow. The time responses of the HESM rotor speed ω, the d-axis current i_d, the q-axis current i_q, and the additional excitation current i_f under the proposed controller and backstepping controller are shown in Figure 1. The time responses of the HESM rotor speed error surface S_1, the d-axis current error surface S_2, the q-axis current error surface S_3, and the additional excitation current error surface S_4 are shown in Figure 2 under the proposed controller and backstepping controller.

It is evident from these figures that the proposed control law enhances dynamic performance more than the backstepping technique. Figure 2 shows that, in contrast to backstepping, all error surfaces S_1, S_2, S_3, and S_4 of the proposed control can quickly converge to zero. It is clear that dynamic (transient) performances, such as rapid decrease of oscillatory overshoot and reduced settling time, are improved for certain time responses. It should be emphasized that, although the backstepping controller can satisfy the requirements stated in the paper's goal, it performs worse during transients than the suggested controller. The simulation results ultimately show that the suggested strategy works better than the backstepping methods. Additionally, it has an acceptable dynamic performance, as shown by the quick dampening of oscillations across all time trajectories. It is evident that the reference rotor speed ω_r can be tracked by the HESM rotor speed. Additionally, all closed-loop dynamics signals are constrained by the suggested control approach.

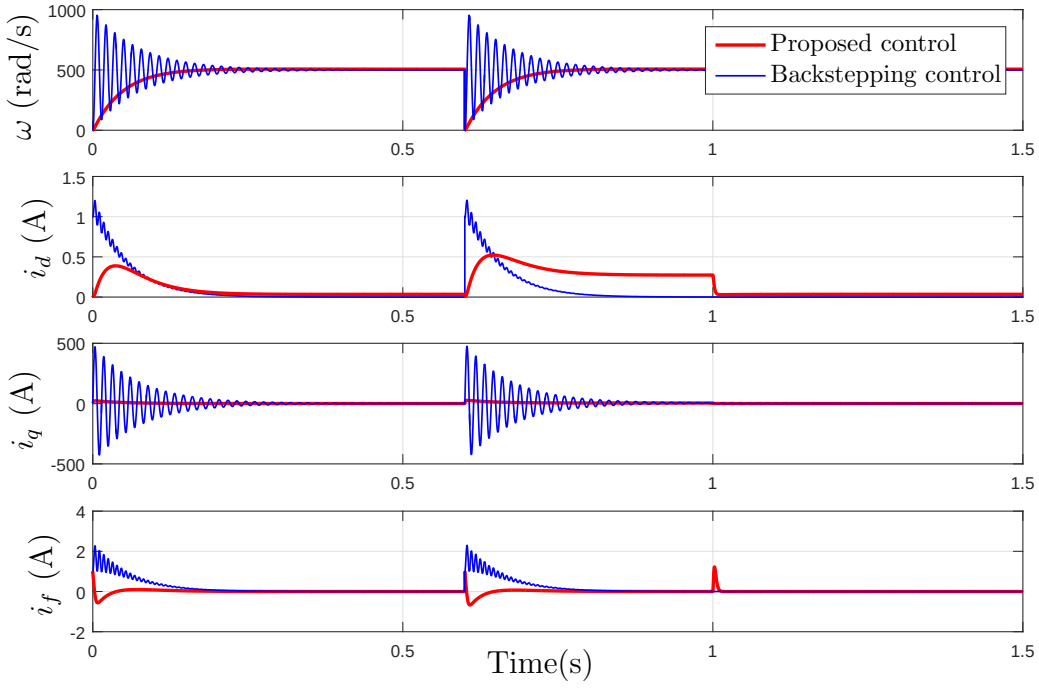

FIGURE 1. Controller performance – Rotor speed ω, d-axis current i_d, q-axis current i_q and additional excitation current i_f under the proposed controller and backstepping controller

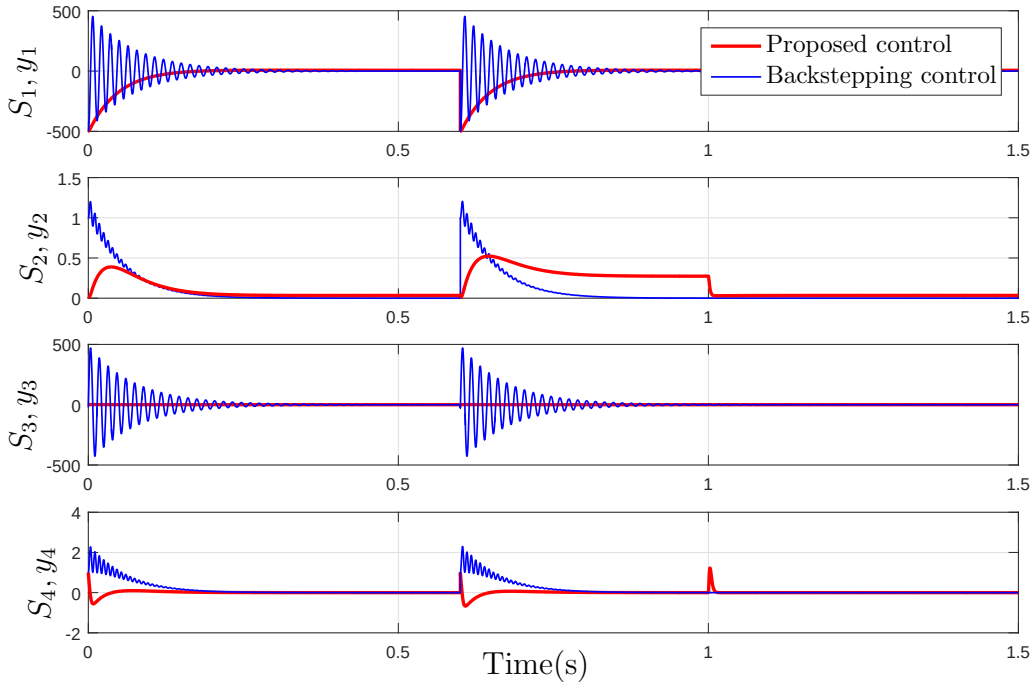

FIGURE 2. Controller performance – Time responses of rotor speed tracking error $S_1 = x_1 - \omega_r$, d-axis current tracking error S_2, q-axis current tracking error S_3 and additional excitation current tracking error S_4 under the proposed controller and backstepping controller

The quantitative results demonstrating the percentage overshoot and the settling time of the rotor speed responses of both the proposed and backstepping controllers are as follows to demonstrate the efficacy of the developed method: It has been found that the proposed method has a percentage overshoot of around 5.09%, while the backstepping method has a percentage overshoot of around 90.6%. Furthermore, the proposed method has a setting time of 0.26 seconds, whereas the backstepping method has a setting time of around 0.48 seconds. Based on these findings, it is easy to conclude that the designed controller outperforms the backstepping design.

In practice, it is well known that it is impossible to create a perfect dynamic model of the system under consideration. It must therefore look into how robust the suggested controller is to changes in system parameter. For the robustness investigation of the developed controller, the system parameter variation must be taken into account. Particularly, the system's parameter, or moment of inertia J, can be uncertain. In addition, it can be challenging to determine the exact value. Therefore, it is important to evaluate how robust the resulting controller is to this variation.

A test of robustness was conducted by changing the parameter from its nominal value, i.e., the moment of inertia J. Specifically, a $\pm 30\%$ variation in the value of J is taken into account in this study. In comparison to the system responses under normal conditions, Figure 3 demonstrates that the proposed scheme can still provide consistent control performance despite system parameter variation. The obtained controller is therefore insensitive to parameter variation.

Remark 4.1. *It is well known that the HESM is a multivariable, strongly coupled, and extremely nonlinear system despite the robustness test's study. The coupling between speed*

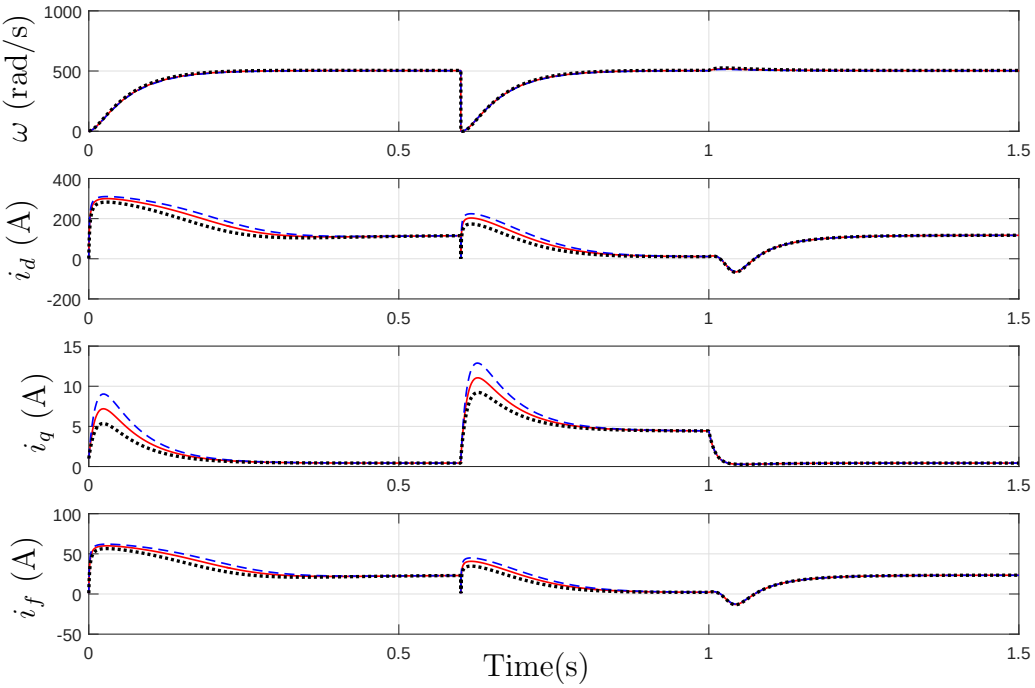

FIGURE 3. Controller performance – Rotor speed ω, d-axis current i_d, q-axis current i_q and additional excitation current i_f under the parameter variation of the moment of inertial (Solid: nominal value, Dashed: +30%, Dashdotted: −30%)

and armature currents, as well as disturbances like inaccurate modeling of uncertain parameters (armature winding resistance, moment of inertia, etc.), sensor errors (angular position, angular velocity), and discretization influences, are the main causes of the high nonlinearity (delay, numerical errors). The HESM controller should be completely designed with the adaptive control laws overcoming the unknown parameters, in particular the moment of inertia J, friction coefficient R_Ω, and the load torque T_l, which will be reported in the future, in order to deal with the high nonlinearity.

In conclusion, the simulation results demonstrate that the proposed method outperforms both the backstepping design. Also, it provides satisfactory dynamic performance, as demonstrated by the rapid damping of oscillations across all time trajectories. Clearly, the HESM rotor speed is able to track the reference rotor speed ω_r. In addition, with the proposed control strategy, all closed-loop dynamics signals are semi-globally uniformly ultimately bounded.

5. **Conclusion.** The dynamic surface control technique has been used to design the nonlinear controller in this study. The simulation results indicate that the proposed control mechanism works well. It can not only keep all signals of closed-loop system trajectories stable and all semi-globally uniformly ultimately bounded, but it can also rapidly converge to zero according to the desired requirements. The presented approach outperforms the backstepping method in terms of improved dynamic control performance. Furthermore, the results show that the proposed controller is effective at addressing the rotor speed tracking problem and improving transient performance in the face of abrupt load torque changes. Future research will concentrate on how to put this strategy into action in order

to develop an adaptive backstepping nonsingular terminal sliding mode method [16] for the HESM model with unknown parameters.

REFERENCES

[1] Y. P. Dou, *Design Research of Hybrid Excitation Synchronous Generator*, Ph.D. Thesis, Nanjing University of Aeronautics and Astronautics, Nanjing, China, 2002.

[2] C. Zhao and Y. Yan, A review of development of hybrid excitation synchronous machine, *Proc. of the IEEE International Symposium on Industrial Electronics*, Dubrovnik, Croatia, pp.857-862, 2005.

[3] S. Hlioui, Y. Amara, E. Hoang, M. Lecrivain and M. Gabsi, Overview of hybrid excited synchronous machines technology, *Proc. of 2013 International Conference on Electrical Engineering and Software Applications*, Hammamet, Tunisia, pp.1-10, 2013.

[4] S. Hlioui, M. Gabsi, H. B. Ahmed, G. Barakat, Y. Amara, F. Chabour and J. J. H. Paulides, Hybrid excited synchronous machines, *IEEE Transactions on Magnetics*, vol.58, no.2, 2022.

[5] Q. Xie, Z. Han and H. Kang, Adaptive backstepping control for hybrid excitation synchronous machine with uncertain parameters, *Expert Systems with Applications*, vol.37, pp.7280-7284, 2010.

[6] G. Rigatos, P. Siano, P. Wira, M. Abbaszadeh and V. Ambrozic, Nonlinear $\mathcal{H}_\infty$ control for hybrid excited synchronous generators, *Proc. of 2020 IEEE 14th International Conference on Compatibility, Power Electronics and Power Engineering (CPE-POWERENG)*, Setubal, Portugal, pp.273-278, 2020.

[7] X. Sun, L. Meng, J. Liang and S. Li, Hybrid excitation synchronous motor feedback linearization decoupling sliding mode control, *Proc. of 2019 22nd International Conference on Electrical Machines and Systems (ICEMS)*, Harbin, China, 2019.

[8] M. Krstic, I. Kanellakopoulos and P. Kokotivic, *Nonlinear and Adaptive Control Design*, John Wiley & Sons, New York, 1995.

[9] D. Swaroop, J. K. Hedrick, P. P. Yip and J. C. Gerdes, Dynamic surface control for a class of nonlinear systems, *IEEE Transactions on Automatic Control*, vol.45, no.10, pp.1893-1899, 2000.

[10] P. P. Yip and J. K. Hedrick, Adaptive dynamic surface control: A simplified algorithm for adaptive backstepping control of nonlinear systems, *International Journal of Control*, vol.71, no.5, pp.959-979, 1998.

[11] Z. J. Yang, K. Miyazaki, S. Kanae and K. Wada, Robust position control of a magnetic levitation system via dynamic surface control technique, *IEEE Transactions on Industrial Electronics*, vol.51, no.1, pp.26-34, 2004.

[12] D. Chwa, Global tracking control of underactuated ships with input and velocity constraints using dynamic surface control method, *IEEE Transactions on Control Systems Technology*, vol.19, no.6, pp.1357-1370, 2011.

[13] Y. H. Chang and W. S. Chan, T-S fuzzy model-based adaptive dynamic surface control for ball and beam system, *IEEE Transactions on Industrial Electronics*, vol.60, no.6, pp.2251-2263, 2013.

[14] J. Yu, P. Shi, W. Dong, B. Chen and C. Lin, Neural network-based adaptive dynamic surface control for permanent magnet synchronous motors, *IEEE Transactions on Control Systems Technology*, vol.23, no.6, pp.640-645, 2015.

[15] A. Kanchanaharuthai and E. Mujjalinvimut, Adaptive dynamic surface control for higher-order model of synchronous generators, *International Journal of Innovative Computing, Information and Control*, vol.16, no.2, pp.749-794, 2020.

[16] Q. Zhu, J. Wang and Y. Zhu, Adaptive backstepping nonsingular terminal sliding mode control of servo system based on new sliding mode and reaching law, *International Journal of Innovative Computing, Information and Control*, vol.18, no.6, pp.1689-1700, 2022.

Author Biography

Ekkachai Mujjalinvimut received the B.Eng., M.Eng. and D.Eng. degrees in the Department of Electrical Engineering from King Mongkut's University of Technology Thonburi (KMUTT), Bangkok, Thailand, in 2007, 2009 and 2016, respectively. He is currently an Assistant Professor at the Department of Electrical Engineering, KMUTT, Thailand. His current research interests include switched mode power supplies, and digital control of power electronic converters together with power system stability and control.

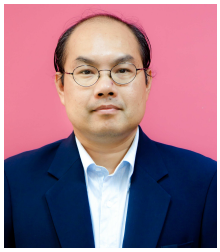

Adirak Kanchanaharuthai received the B.Eng. degree in Control Engineering from King Mongkut's Institute of Technology Ladkrabang, Thailand, the M.Eng. degree in Electrical Engineering from Chulalongkorn University, Thailand, and the Ph.D. degree in Systems and Control Engineering from Case Western Reserve University, Cleveland, OH, USA, in 1995, 1997, and 2012, respectively. Currently, he is an Associate Professor at the Department of Electrical Engineering, Rangsit University, Thailand. His main research interests include power system dynamics, stability and control, renewable energy systems, energy storage systems, and applications of nonlinear control theory to power systems, flexible alternating current transmission systems (FACTS) devices, and congestion tracking control for TCP/AQM network systems.